Effect of changes in relative humidity on aerosol scattering near clouds

Cynthia H. Twohy,[1] James A. Coakley Jr.,[1] and William R. Tahnk[1]

Received 15 August 2008; revised 8 December 2008; accepted 30 December 2008; published 6 March 2009.

[1] Many investigations using satellite data have determined that aerosol optical depth and cloud cover are correlated and some have interpreted the correlation as evidence of an aerosol indirect effect on clouds. This study uses in situ aircraft observations taken during the Indian Ocean Experiment (INDOEX), February–March 1999, and mostly over the northern Indian Ocean, to show that on average, relative humidity increases as distance to the boundaries of small marine trade cumulus decreases. The increase is sufficient to cause substantial growth of hygroscopic aerosol particles and consequently greatly enhance particle scattering cross sections near clouds. The measured increase is from a relative humidity of about 90% at 1-km horizontal distance from the cloud to about 94–96% at 100 m from cloud edge. This increase would result in about a 40–80% increase in aerosol scattering cross section based on the composition used to model the aerosol. Observations of scattering in the vicinity of clouds using 30-m-resolution imagery from the Multichannel Cloud Radiometer (MCR) indicated that the increase in scattering within 1–2 km of cloud edge was about 50%, comparable to the increase calculated for the particle scattering cross sections. On the basis of these findings, global average estimates of the aerosol direct radiative effect as derived from satellite observations of cloud-free oceans is estimated to be 35–65% larger than that inferred for large (>20 km) cloud-free ocean regions. This enhancement is consistent with those derived from satellite observations.

Citation: Twohy, C. H., J. A. Coakley Jr., and W. R. Tahnk (2009), Effect of changes in relative humidity on aerosol scattering near clouds, *J. Geophys. Res.*, *114*, D05205, doi:10.1029/2008JD010991.

1. Introduction

[2] Satellite observations are increasingly being used to infer indirect effects of aerosols from correlations of aerosol and cloud properties in localized regions [e.g., *Kaufman and Nakajima*, 1993; *Kaufman and Fraser*, 1997; *Wetzel and Stowe*, 1999; *Nakajima et al.*, 2001; *Sekiguchi et al.*, 2003; *Quaas et al.*, 2004; *Kaufman et al.*, 2005; *Matheson et al.*, 2005, 2006a; *Quaas et al.*, 2008; *Loeb and Schuster*, 2008]. These studies relate some indicator of aerosol loading, such as total optical depth [*Kaufman and Fraser*, 1997] or derived fine particle column number [*Nakajima et al.*, 2001], to regional cloud properties. Many of these investigations have determined that aerosol burdens increase as regional cloud cover increases. Some have attributed this positive correlation as evidence for the longer cloud lifetimes expected for increased aerosol number, reduced droplet size, and reduced drizzle or precipitation as hypothesized by *Albrecht* [1989]. On the other hand, aerosol burdens and cloud cover can increase together owing to a number of physical processes, some of which are unrelated to the effects of aerosols on clouds [*Matheson et al.*, 2005]. Estimates of both the direct and the indirect radiative forcing by aerosols are hampered because aerosol properties change as they move from largely cloud-free regions into cloudy environments. In addition, with regard to the indirect effect of aerosols, satellite observations of cloud fractions, cloud optical depths, and droplet radii become error-prone in partly cloudy environments [*Matheson et al.*, 2006b]. Currently, these effects are not well quantified and are poorly accounted for, if at all, in estimates of both the aerosol direct and indirect radiative forcings.

[3] The following factors may affect the remote sensing results and their interpretation in partly cloudy regions: (1) residual cloudiness (cloud contamination) of imagery pixels identified as cloud-free that lie within broken cloud systems, (2) enhanced reflectivity of cloud-free columns due to the scattering of sunlight reflected by nearby clouds [*Podgorny*, 2003; *Wen et al.*, 2007; *Marshak et al.*, 2008], (3) hygroscopic growth of particles that results from the elevated relative humidity of the cloudy environment [*Clarke et al.*, 2002], (4) enhanced particle size resulting from the chemical processing of solutes within clouds that subsequently dissipate [*Hoppel et al.*, 1986], and (5) new particle production in detraining regions of clouds [*Twohy et al.*, 2002]. The first two factors may cause apparent increases in aerosol optical depth in partly cloudy regions, which are unrelated to either the aerosol direct or indirect effects. The last three factors can cause actual aerosol optical depth increases that increase as cloudiness increases. These latter processes, however, would not be the result of

[1]College of Oceanic and Atmospheric Sciences, Oregon State University, Corvallis, Oregon, USA.

0148-0227/09/2008JD010991

Table 1. Summary of Cloud Penetrations Analyzed in This Study

INDOEX Flight Number (Date)	Flight Objective	Number of Flight Legs Encountering Clouds	Number of Clouds	Extent of Flight Legs	
				Latitude	Longitude
4 (24 Feb)	Cross equatorial	10	28	4.6°S to 3.3°N	73.2°E to 73.4°E
6 (27 Feb)	Polluted cloud bands	10	26	6.3°N to 8.9°N	66.2°E to 66.8°E
9 (7 Mar)	Clean and polluted clouds	17	35	4.0°N to 12.0°N	63.7°E to 73.5°E
12 (13 Mar)	Polluted clouds	11	50	5.4°N to 8.2°N	70.2°E to 73.1°E
13 (16 Mar)	Polluted clouds	6	38	6.5°N to 13.4°N	67.0°E to 71.8°E
14 (18 Mar)	Clean and polluted clouds	6	43	0.8°S to 3.7°N	70.9°E to 72.3°E
16 (21 Mar)	Polluted clouds	7	58	5.1°N to 10.9°N	67.8°E to 73.5°E
17 (24 Mar)	Cross equatorial	1	29	6.1°S to 6.4°S	71.2°E to 72.5°E
18 (25 Mar)	Moderately polluted clouds	8	39	4.0°N to 7.0°N	73.5°E to 87.5°E

indirect effects of aerosol particles on cloud properties, but rather the converse: cloud effects on aerosol properties.

[4] This study focuses on changes in relative humidity and aerosol particle number in cloud-free regions adjacent to clouds as a function of the distance from the cloud boundaries. It sets out to characterize changes others have previously noted. For example, using in situ observations, *Radke and Hobbs* [1991] and *Lu et al.* [2003] reported enhanced humidity around some cumulus clouds and termed these regions cloud "halos." The halos were observed over both land and water and extended up to a few kilometers from the cloud boundary itself. The investigators attributed the halos to turbulent mixing and evaporation of droplets near cloud edges. From satellite measurements, *Charlson et al.* [2007] observed a continuum of reflectances at visible wavelengths between clear and cloudy states in the atmosphere. *Koren et al.* [2007] found that optical depths obtained with the Aerosol Robotic global Network (AERONET) decreased and Ångström exponents increased (indicating smaller particles) with time after the passage of clouds. They also reported that reflectances of cloud-free ocean regions at 870 nm obtained with the Moderate Resolution Imaging Spectrometer (MODIS) increased as distances decreased from 30 km to the edges of clouds. This study seeks to quantify the extent to which changes in relative humidity and changes in particle concentrations and the consequent effects on the aerosol scattering cross section can explain the observed changes in scattered light near clouds.

[5] The study uses observations made primarily using the National Center for Atmospheric Research (NCAR) C-130 during the Indian Ocean Experiment (INDOEX) in February and March 1999. The focus is on low-level marine cumulus. On extended flight legs that penetrated the cumulus clouds, particle counts and relative humidity were measured between clouds. Estimates of the enhancement in scattering cross sections were derived for an externally mixed model of the INDOEX aerosol that has been used to model aerosol scattering [*Rajeev et al.*, 2000]. High spatial resolution images of broken clouds collected with the Multichannel Cloud Radiometer (MCR), also flown on the C-130 during INDOEX, show enhancements in scattering that are similar in character to those predicted for the aerosol scattering cross sections. CALIPSO lidar observations are then used to derive sizes of cloud-free ocean regions, and the sizes, together with the enhancements in aerosol scattering cross sections, are used to estimate the effects of the increase in relative humidity (RH) on the aerosol direct radiative effect for oceans. The aerosol direct radiative effect is the difference in the albedos of cloud-free oceans and that inferred for both cloud-free and aerosol-free oceans. The estimates obtained in this study are compared with those derived from satellites by *Loeb and Manalo-Smith* [2005] and by *Koren et al.* [2007].

2. Observations

[6] Both in situ and remotely sensed observations were collected by the NCAR C-130 aircraft during the 1999 intensive field phase of INDOEX. Small cumulus clouds were sampled in polluted air downwind of India as well as in clean air south of the Intertropical Convergence Zone [*Ramanathan et al.*, 2001]. In addition to in situ thermodynamic, moisture, and particle measurements, high spatial resolution MCR imagery and the Scanning Aerosol Backscatter Lidar (SABL) observations were also collected. Here the analysis is focused on the in situ thermodynamic and particle observations, with representative samples of the MCR imagery illustrating changes in aerosol scattering comparable to those estimated on the basis of the in situ measurements.

[7] The C-130 data were searched for constant low-level flight legs (below 1.5 km) that penetrated clouds and where all instruments were functioning. Nine research flights in both polluted and clean air yielded legs suitable for analysis. The samples collected under clean conditions, particle concentrations less than 500 cm^{-3} as obtained with a Thermo-Systems Inc. Model 3760 condensation nucleus (CN) counter, represented less than 10% of the cases, too few to allow comparisons of the effects for clean and polluted clouds. Table 1 lists the flights that yielded clouds in this study. Figure 1 shows the locations of the flights. Data sampled every second in air between clouds was composited to reveal trends in relative humidity and particle concentrations as a function of distance to the actual cloud boundaries. The results are for all of the clouds, both polluted and clean, but owing to the paucity of the clean samples, they should be interpreted as being dominated by polluted clouds.

[8] Humidity data was from the cross-flow Lyman-alpha hygrometer [*Friehe et al.*, 1986]. The Lyman-alpha sensor, while fast in response, is prone to electronic drift, and is loosely coupled to the more stable General Electric dew point hygrometer to provide more accurate absolute humidity values [*Schanot*, 1987]. Using the 1 Hz Rosemount temperature probe for an ambient temperature value, absolute humidity was converted to relative humidity for the data presented here. An offset of about 1% occurred in the

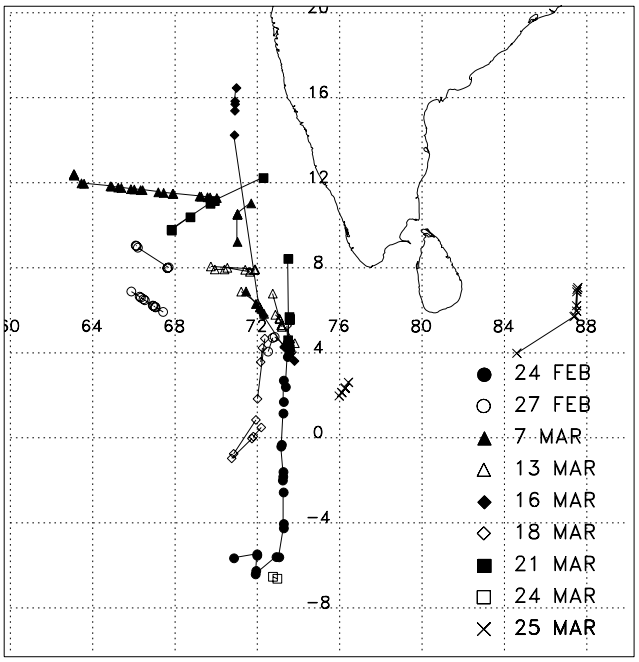

Figure 1. Locations of cloud-penetrating flight legs that yielded observations used in this study.

mean Lyman-alpha data relative to the mean out-of-cloud dew point data, and the mean in-cloud value was 102.7%. The uncertainty of the mean relative humidity data is therefore estimated to be about 2% when both bias and random errors are considered. Here, however, greater emphasis is placed on departures from the mean humidity.

[9] Three different types of aerosol probes were used to examine changes in aerosol concentration as a function of distance from cloud entry. The Particle Measurement Systems (PMS) Forward-Scattering Spectrometer Probe (FSSP)-300 measures the size distribution of particles between about 0.3 μm and 20 μm diameter [*Baumgardner et al.*, 1992] while the PMS Passive Cavity Aerosol Spectrometer Probe PCASP-100 measures sizes between $\sim$0.1 μm and 3.0 μm diameter. Both probes are located outside the aircraft on the wing. The FSSP-300 has no inlet and so has minimum disturbance upstream of the sample volume. The PCASP, on the other hand, has a small heated inlet, so particles are dried before measurement [*Strapp et al.*, 1992]. The Thermo-Systems CN counter was used to determine total particle concentrations. The counter condenses butanol vapor on all particles larger than about 0.01 μm diameter so that they grow to an optically detectable size.

[10] "In-cloud" air was determined using particle concentrations from a PMS FSSP-100, which measures concentrations for particles with diameters ranging from 3 μm to 45 μm, and liquid water concentrations from a PMS King probe. Clouds were defined as regions where the droplet concentration was >10 cm^{-3} and the liquid water concentration was >0.03 g m^{-3} for a period of at least three consecutive seconds ($\sim$330 m). Examples of clouds surpassing these thresholds are shown in Figure 2. Using the same thresholds but requiring that the criteria be met for six consecutive seconds instead of three, had no substantial effect on the results reported in the next section.

[11] Finally, an attempt was made to estimate the consequences of the changes in relative humidity and particle concentrations in the vicinity of clouds on the aerosol direct radiative effect. The estimate required the occurrences of cloud-free distances to cloud for oceans. The distances were obtained using the CALIPSO Vertical Feature Mask, which in turn is derived from the lidar backscatter returns (CALIOP Algorithm Theoretical Basis Document, Part 3: Scene Classification Algorithms available at http://www-calipso.larc.nasa.gov/resources/pdfs/PC-SCI-202_Part3_v1.0.pdf). CALIPSO orbits the Earth as part of the A-Train constellation of satellites, with the lidar sampling a nadir path every 300 m with a beam width of 70 m [*Winker et al.*, 2006]. Cloud-free distances to clouds were derived from daytime observations collected for ocean regions from 60°S to 60°N covering a 15-month period, January 2007 to March 2008.

3. Analysis of In Situ Observations

3.1. Relative Humidity

[12] Figure 2 shows two examples of the changes in relative humidity (RH) during level flight as the aircraft approached and flew through small low-level cumulus clouds. In general, humidity increased between clouds and near the cloud boundaries, as shown in Figure 2 (top). In

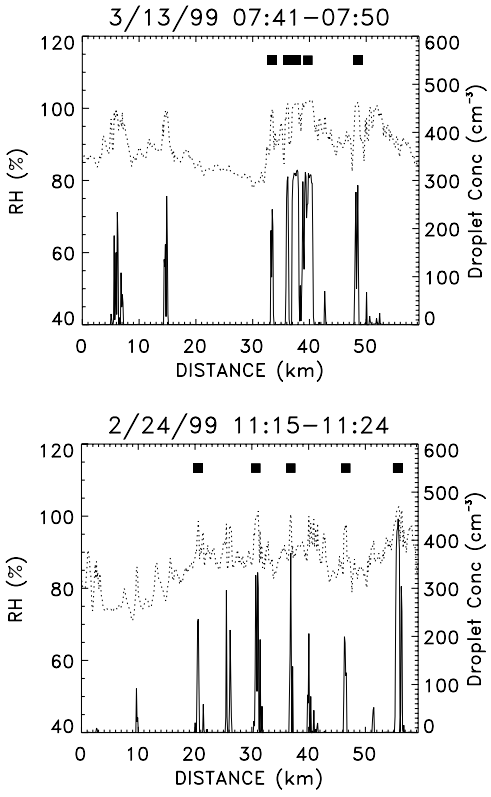

Figure 2. Example of relative humidity (dashed line) obtained with the Lyman-alpha sensor and droplet concentration (solid line) obtained with the FSSP-100 for two different C-130 flight legs at the levels of low-lying clouds during INDOEX. The solid boxes at the top of each plot identify the "in cloud" portions of the flight leg as defined using the criteria described in the text.

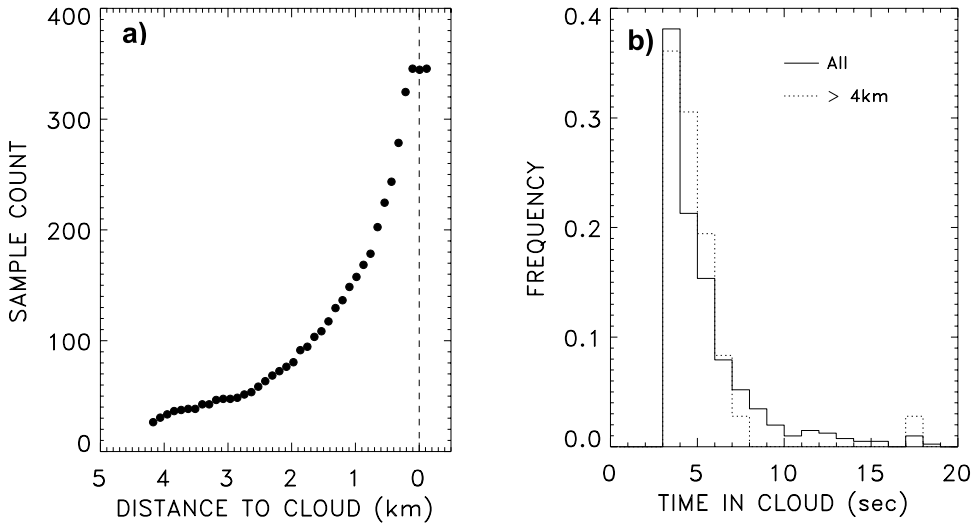

Figure 3. (a) Number of cloud penetrations with a given distance to cloud edge. (b) Time "in cloud." Each second in cloud is about 110 m. In-cloud times are given for clouds with cloud-free lengths to cloud of 110 m (All) and greater than 4 km.

some cases, however, the response was less apparent (Figure 2, bottom). The SABL lidar (data not shown) showed increases in relative backscatter near and between clouds that were often, but not always, correlated with increases in the measured relative humidity.

[13] Owing to the variability in RH illustrated in Figure 2, and also in the particle concentrations discussed later, data from nine different flights were composited to reveal the behavior of the RH and particle fields as a function of distance from cloud entry. The compositing was performed as follows: Flight legs were divided into segments that were centered on individual clouds. A cloudy flight segment was taken to have three parts, an entering cloud-free leg prior to encountering the upstream cloud edge, the in-cloud portion of the leg, and an exiting cloud-free leg after leaving the downstream cloud edge, where upstream and downstream were relative to the aircraft flight track. Cloud edges were the first and the last second of data that satisfied the "in-cloud" criteria given above. The analysis was designed so that the entering and exiting legs were equal in duration. All cloud observations were limited to those with altitudes between 600 m and 1000 m. While analyses were performed for both the entering and exiting legs, results are presented only for the entering legs. Known effects from instruments passing through cloud, such as high residual RH in the dew point hygrometer, low temperatures from the wetting of the temperature probe, and high CN counts, affected the exiting cloud-free observations when compared with the entering observations. For example, the RH obtained with the dew point hygrometer for the exiting legs averaged 2–3% higher than for the entering legs for the kilometer adjacent to the clouds, and the average CN count was over 1500 cm^{-3} higher upon exiting than upon entering, owing to the residual effects of droplet breakup in the inlet [*Weber et al.*, 1998]. Departures of the RH and particle concentrations from the mean for the entering leg were composited for all flights as a function of distance to cloud edges. Figure 3 shows the number of cloud penetrations for the composites as a function of the length of cloud-free air flown through prior to entering the cloud and the distribution of time spent "in cloud." The time in cloud shows that the low-level clouds studied here were typically between 300 and 500 m across. Few clouds extended beyond a kilometer in width.

[14] Figure 4a shows average values (symbols) for the departures from the mean RH obtained with the Lyman-alpha sensor for various distances from cloud edge. In Figure 4a separate lines with different symbols show the departures for several different lengths of cloud-free air prior to entering the cloud. The lengths range from as little as ~110 m (All, open circle: one second prior to entering) to lengths greater than 4 km (solid square). Regardless of the distance flown through cloud-free air prior to entering a cloud edge, the RH showed a distinct rise within 1 km of cloud edge. The distribution of time in cloud shown in Figure 3 suggests that the rise in RH is typical of the smaller clouds studied here (3 s, 300–400 m), as opposed to influences of clouds that might lie on either side of the flight path. The rise in RH was approximately 8% with approximately half of the rise occurring within the last 100 m before cloud edge. No further rise is observed between 1 and 4 km; however, the limited sample of flight legs with larger segments of cloud-free air to cloud edge precluded reliable estimates of cloud-level relative humidity at greater distances. The average RH for the ensemble was 88–90% at a distance of 4 km from cloud edge. In section 4, the rise in scattering expected for the INDOEX aerosol will be considered as the rise in RH climbs from a low of 70–80% in cloud-free regions 20 km from cloud edge to ~90% between 4 km and 1 km from cloud edge and then to ~100% at cloud edge.

3.2. Particle Concentrations

[15] Figures 4b–4d show departures for the particle concentrations. All three particle counting instruments show no significant changes in particle concentrations near clouds, except for within 100 m of cloud edge. Near the cloud edge the concentrations for the PCASP fall while those for the FSSP-300 rise. This behavior is typical of "in-

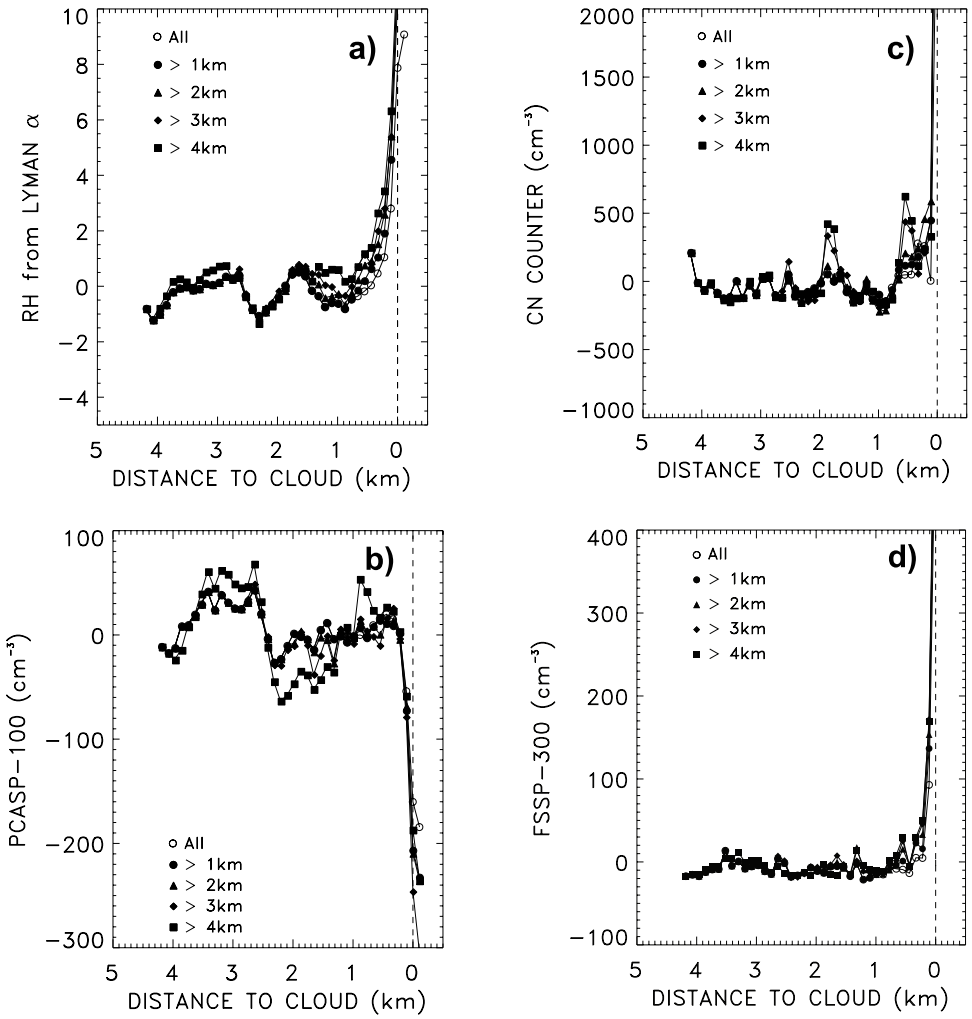

Figure 4. Average departures from the means for flight legs entering clouds for the cloud-free portions composited for all INDOEX flight legs encountering low-level clouds. The departures are for (a) relative humidity, (b) particle concentrations from the PCASP-100, (c) CN counter, and (d) FSSP-300. Average RH for the flight legs was 88–90%. Average particle concentrations were 900 cm^{-3} for the PCASP, 2500 cm^{-3} for the CN counter, and 30–40 cm^{-3} for the FSSP-300. The distances are from the cloud edge. Separate lines show values for different lengths of cloud-free air prior to cloud edge ranging from ~110 m (All) to 4 km.

cloud'' values, where the PCASP concentrations (particle diameters 0.1–3.0 μm) decrease owing to the transfer of particles out of the upper size ranges into cloud droplet sizes. The FSSP-300 particle concentrations (diameters 0.3–20 μm) rise owing to the growth of particles from below the lower size range of the probe into the detected size range, either through the swelling of haze particles or the nucleation of cloud droplets. The increase, however, could also be caused by the remnants of clouds at cloud edges. These remnants surpassed the particle concentration and liquid water concentration thresholds for clouds but failed to sustain the required levels for the 3-s period invoked as being ''in cloud.''

4. Effects of Increasing RH on Aerosol Scattering Cross Sections

[16] The aerosol scattering cross sections were calculated using the chemical composition of the INDOEX aerosol as deduced from C-130 and surface-based observations and described by *Rajeev et al.* [2000]. The particle growth in response to increasing RH followed the prescriptions given by *Hess et al.* [1998]. The aerosol is treated as being externally mixed. According to Rajeev et al., 20% of the INDOEX aerosol by number concentration is water soluble: sulfate, nitrate, ammonia, and organics, and 80% is soot. In addition there are small number concentrations of sea salt, which is soluble, and mineral dust, which is not. When considering the effects of RH on aerosol scattering, values of 70% and 80% were chosen for regions far from clouds on the basis of perusal of the C-130 flight legs in cloud-free air at the same altitudes of the low-level clouds but at distances greater than 30 km from clouds.

[17] Figure 5 shows calculated increases in the aerosol scattering cross section as a function of increasing RH from 70 to 99% relative to its value at 70%. Even though the RH rises only 4–6% as distances fall from 1 km to 100 m of cloud edge, the consequence of this rise, as shown in

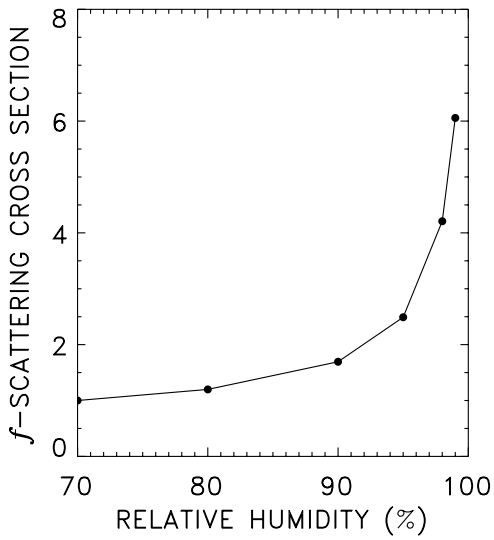

Figure 5. Ratios of scattering cross sections for INDOEX aerosol and relative humidity, normalized by the value at a relative humidity of 70%.

Figure 5, would be about a 40–80% increase in the scattering cross section, taking 90% as the initial RH at 1 km. Since the reflectances used to infer aerosol optical depths from satellite imagery are proportional to the scattering cross sections, the increase would suggest a comparable increase in aerosol optical depth and in estimates of the aerosol direct radiative effects, provided that the increases in RH and scattering cross sections occurred throughout the aerosol layer, which is unlikely. On the basis of the findings of *Feingold and Morley* [2003], the rise in RH and scattering cross section would be confined to the atmosphere near the cloud level, and thus only a portion of the aerosol column would be affected to the degree shown in Figure 5. Perusal of SABL lidar backscatter returns suggests that the fraction of particles affected would be about one quarter to one third for the low-level clouds studied in INDOEX. With a quarter of the aerosol column affected by the rise in RH, the increase in scattering cross sections would be reduced accordingly, to 10–20%.

[18] Finally, when considering an externally mixed aerosol, as is done here, more than 90% of the scattering is contributed by the water soluble components when the RH is 70% or greater. As a result, the fractional increase in scattering cross section is remarkably independent of aerosol composition. Under the simplifying assumption that the aerosol is externally mixed, the fractional increase for a soluble, nonabsorbing, tropical marine aerosol would differ by no more than a few percent from that for a largely insoluble, polluted, urban aerosol, similar to the INDOEX aerosol. Of course, the rise in RH is accompanied by an increase in particle size and changes in the wavelength dependence of the scattering. The changes in the wavelength dependence, however, are small. For the wavelengths of 0.64 and 1.06 μm and for a 4–6% rise in RH from 90% the fractional increases in scattering cross sections calculated for the INDOEX aerosol differ by less than 5%. Similarly small differences in the wavelength dependence of scattering were calculated for the tropical marine aerosol described by *Hess et al.* [1998]. Such small changes would be difficult to detect in multispectral imagery such as that obtained with the MCR described in section 5.

5. Analysis of MCR Imagery

[19] The MCR is a multichannel, high spatial resolution imager. The nominal pixel resolution is ~30 m when the instrument is flown at an altitude of 5 km. The instrument scans perpendicular to the direction of the flight path to a scan angle of 45° each side of nadir. Four channels at shortwave and near infrared wavelengths worked reliably and with good signal-to-noise ratios during the INDOEX missions. Here radiances from the 0.64- and 1.06-μm channels will be analyzed to reveal the enhancement in reflected radiances near cloud edges. It should be noted that the comparisons of the MCR observations with the in situ observations are only statistical. In only a couple of the INDOEX flights were legs flown so that once clouds had been probed, an overpass was flown to obtain remotely sensed data for the clouds that had just been probed. None of the clouds which contributed observations to this study were part of the combined in situ and remotely sensed flight legs.

[20] Figure 6 shows an image constructed from 0.64-μm radiances obtained with the MCR. The image is for a flight leg in the Southern Hemisphere where the atmosphere was relatively free of aerosol. At the nominal altitude at which MCR data was collected during INDOEX, the image swath is approximately 10 km. Sun glint from the cloud-free ocean surface appears on the left side of the image. The sharp shadows of clouds appearing in the region of Sun glint are evidence of the low turbidity in the Southern Ocean. Figure 7 shows the 0.64- and 1.06-μm radiances obtained for the two narrow strips identified by rectangles in Figure 6. One of the strips shows radiances for the cloud-free region away from Sun glint, on the right side of the image; the other shows radiances that arise when clouds are encountered away from the region of Sun glint. In Figure 7, a rudimentary cloud mask has been applied to distinguish 30-m MCR pixels that are cloud-free from those that contain clouds. MCR pixels were identified as cloud-free if they belonged to a 4 × 4 pixel array for which the standard deviation of the 0.64-μm radiances was less than 2% of the mean value. Cloud-free oceans are spatially uniform on small spatial scales while clouds exhibit considerable variability even on the 30-m pixel scale analyzed here. The radiances shown in Figure 7 identified as cloud-free and cloudy clearly show the difference in variability that marks the presence of clouds. The radiances in Figure 7 reveal that the cloud-free reflectances in the strip that encounters clouds depart significantly from those far from clouds within approximately 50 MCR pixels (~1.5 km) from cloud edge.

[21] Figure 8 shows an image similar to that appearing in Figure 6, but in the Arabian Sea where aerosol burdens were high. In regions of heavy aerosol concentrations, the intensity of scattered light was so high that unlike the distinct shadows shown in Figure 6, those of clouds in turbid regions are somewhat diffuse. Figure 9 shows the 0.64-

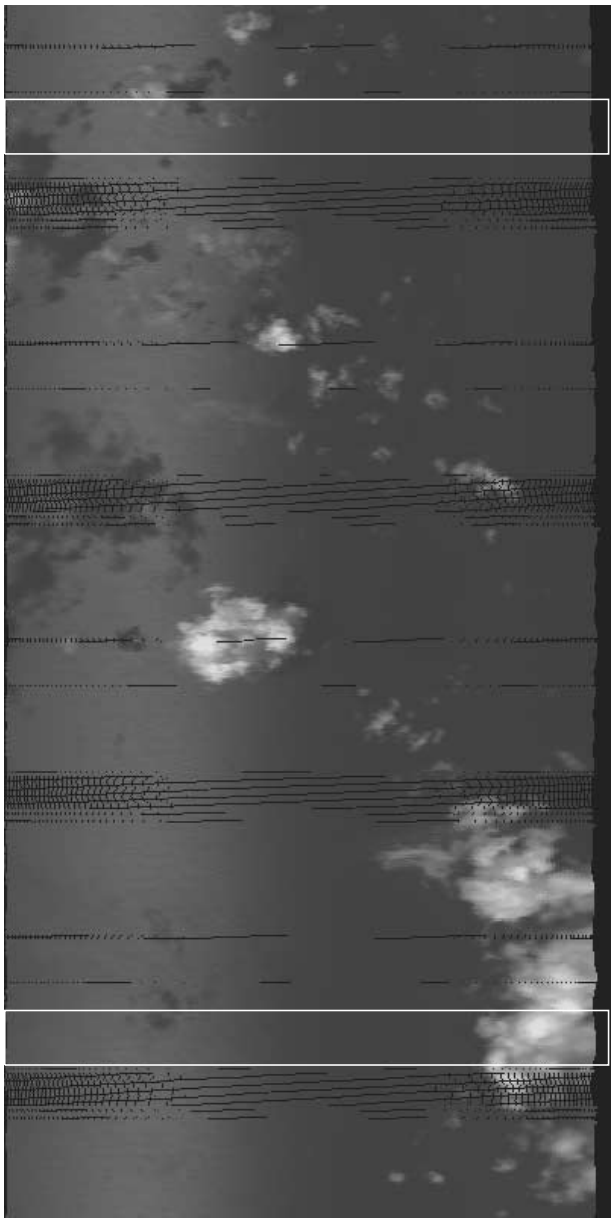

Figure 6. Image constructed from MCR 0.64-μm radiances. The center of the image is at 2.7°S, 73.2°E and was collected during INDOEX flight 4 on 24 February. Aerosol optical depth is relatively low in this scene. The sharp shadows in the region of Sun glint at the left of the image reflect the low aerosol concentrations. The width of the image is approximately 10 km, and the length is approximately 25 km. Data taken from the two rectangular strips outlined in the image are shown in Figure 7. The strips are approximately 1.5 km in width. The strip at the top is largely cloud-free in the portion away from the Sun glint. The strip at the bottom intersects a cloud.

and 1.06-μm radiances for the strip that is cloud-free and for the strip that encounters clouds on the side of the image away from Sun glint. As is the case for the relatively clean atmosphere of the Southern Hemisphere, the radiances at both wavelengths rise significantly starting approximately 1.5 km from the cloud edge.

[22] Unfortunately, the calibrations of the MCR radiances during the INDOEX mission were rather uncertain. Checks of the calibrations obtained using regions of Sun glint in the Southern Hemisphere following methods described by *Luderer et al.* [2005] revealed changes in the relative calibrations of the different channels from flight to flight. Consequently, the following strategy was used to quantify the enhancement of the cloud-free reflectances as cloud edges were approached. The calibrations of both the 0.64- and 1.06-μm channels were assumed to remain constant for all scan lines between the rectangular region that was cloud-free and its counterpart that encountered a cloud edge. The

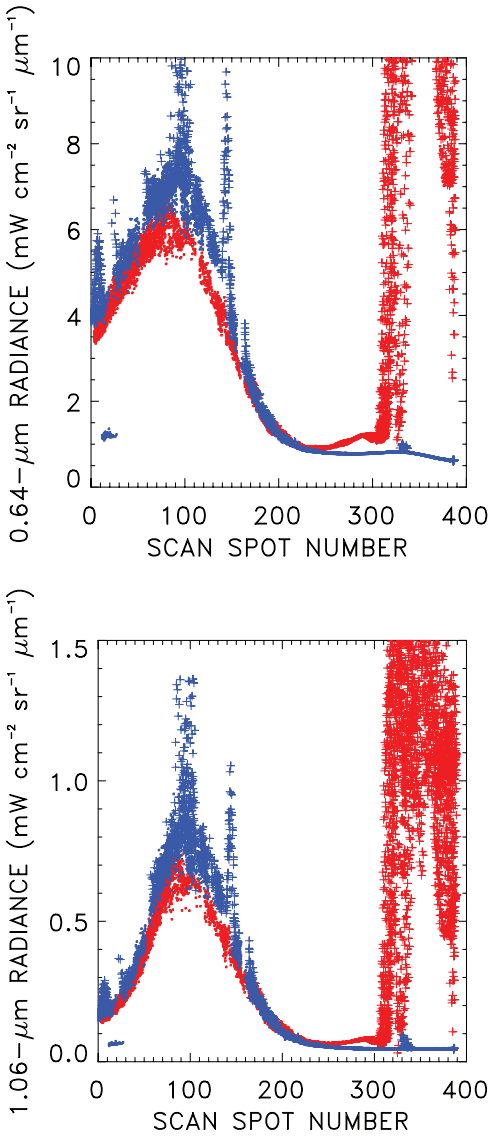

Figure 7. The 0.64- and 1.06-μm radiances for the strips that are cloud-free (blue) and that encounter a cloud (red) as shown in Figure 6. Radiances for 30-m MCR pixels identified as being cloud-free are rendered as dots; pixels identified as containing cloud are rendered with plus signs. A distinct rise in 0.64- and 1.06-μm radiances appears approximately 50 MCR pixels, approximately 1.5 km, prior to encountering the edge of the cloud.

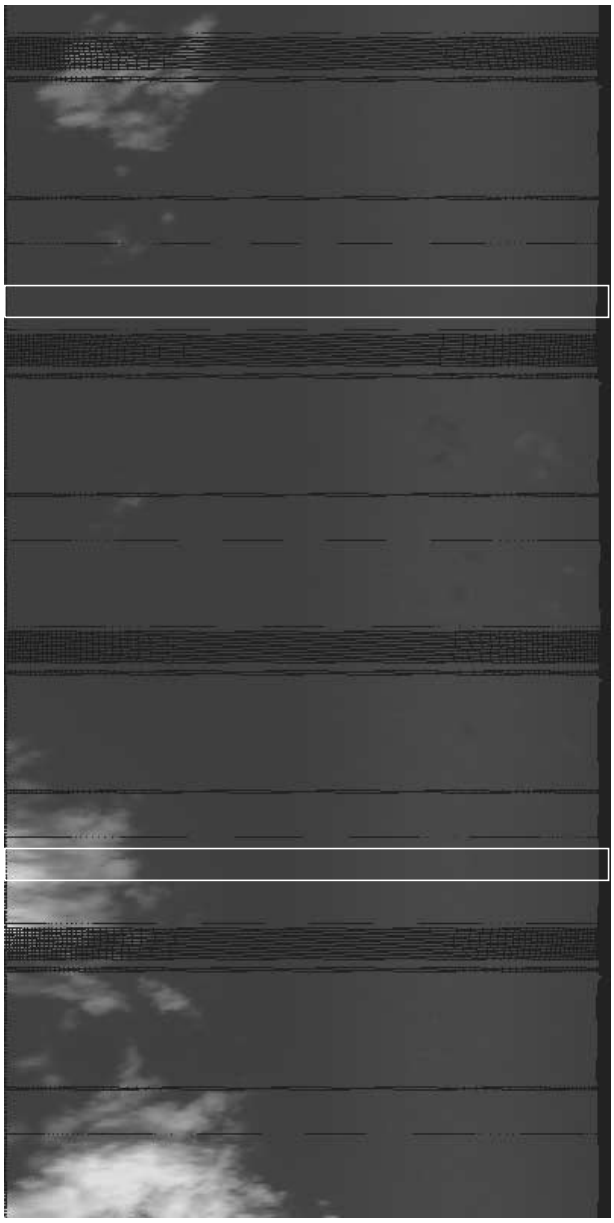

Figure 8. Same as Figure 6 but centered at 8.8°N, 68.0°E and collected during INDOEX flight 5 on 25 February. The aerosol optical depth was relatively large in this region.

departures of the radiances, normalized by the cloud-free values, is given by

$$I_D = \frac{I'_S - I_S}{I_S}, \quad (1)$$

where I'_S represents the cloud-free radiances for the strip that encountered clouds and I_S represents the cloud-free radiances for the cloud-free strip.

[23] Figure 10 shows the enhancement in the cloud-free radiances caused by the presence of cloud expressed as a percentage of the unenhanced background cloud-free reflectance. For both the relatively clean and turbid cases, the enhancement in the reflected cloud-free radiances begins approximately 70 MCR pixels (~2 km) from the cloud edge and reaches approximately 50% at the cloud edge. For the relatively clean case shown in Figure 10a, the fractional change in the 1.06-μm reflectance increased by nearly 70%. The downturn in the scattering enhancement shown in Figure 10a for the clean case is caused by a portion of the cloud-free ocean shadowed by the cloud. While only two examples are presented, other cases with various Sun-target-sensor geometries and clouds provided similar enhancements in the reflectivities of the cloud-free oceans in the vicinity of the clouds. Nonetheless, as the enhancements in scattering should depend on viewing geometry, aerosol type, aerosol loading, and the reflectivities of the clouds being encountered, a thorough investigation of the MCR observations is warranted and remains to be done.

[24] The enhancement in scattering observed with the MCR is comparable in magnitude to the increase in scattering cross section calculated on the basis of the RH data for the last kilometer before cloud edge, provided the increase in RH is assumed to affect all the particles in the

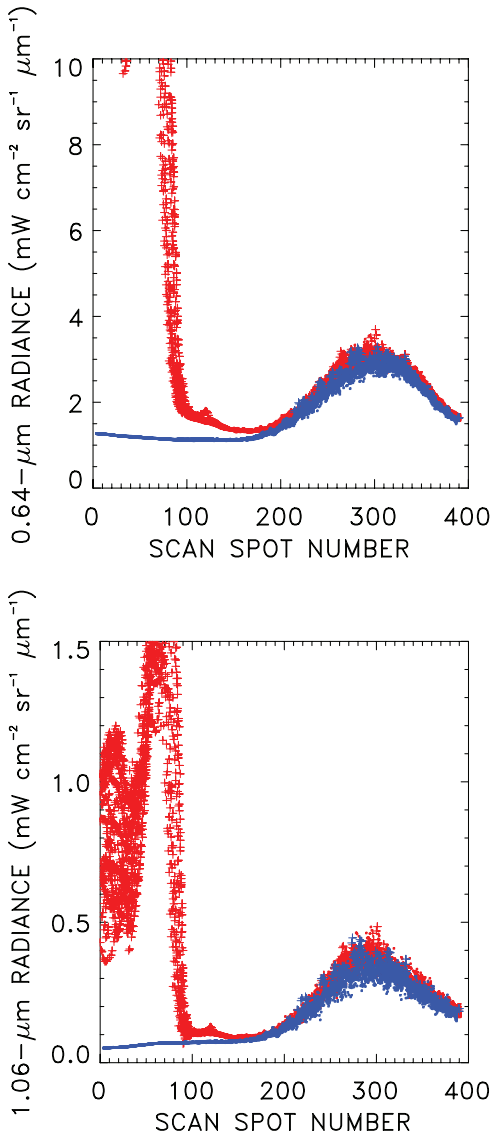

Figure 9. Same as Figure 7 but for the strips that are cloud-free and that encounter clouds in Figure 8.

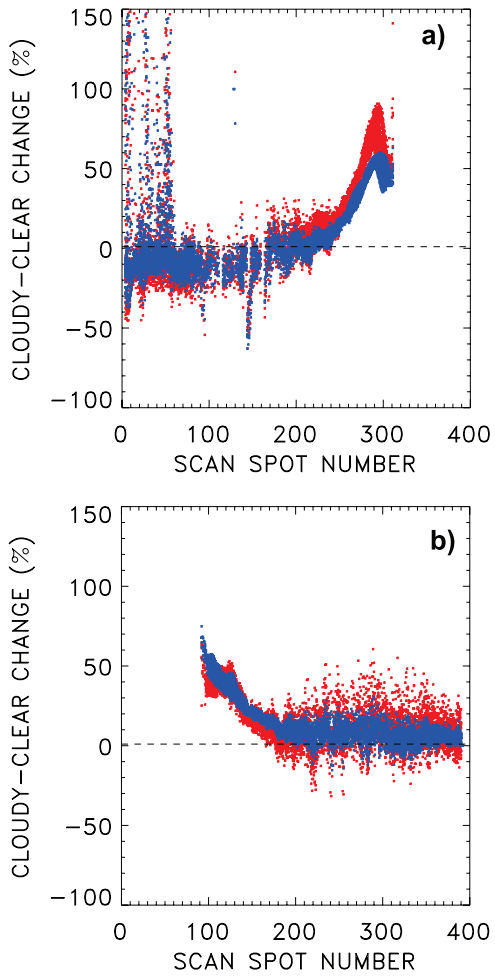

Figure 10. Departures of the 0.64-μm (blue) and 1.06-μm (red) radiances from the cloud-free values expressed as a percentage of the cloud-free values for the strips encountering a cloud as shown (a) in Figure 6 and (b) in Figure 8.

column. As noted in section 4, only a fraction of the column comparable to the cloud thickness is probably affected. In addition, the rise in scattering observed with the MCR begins somewhat earlier (2 km compared with 1 km). The enhancement observed with the MCR includes effects due not only to particle growth but also to the extra illumination of the cloud-free atmosphere that arises from the scattering of sunlight by the nearby clouds [*Marshak et al.*, 2008]. This enhancement includes reflection of the clouds by the underlying ocean surface and scattering of the extra sunlight by the aerosol particles and molecules between the surface and the MCR. Here, no attempt is made to separate the relative magnitudes of these different influences.

6. Implications of Cloud Enhancement in the Aerosol Direct Radiative Effect

[25] To provide context for the INDOEX observations of RH near clouds, the observations were used to roughly estimate cloud enhancements to the aerosol direct radiative effect for cloud-free oceans. Because the enhancements in humidity were limited to the INDOEX clouds, which were largely small marine cumulus, and because the model used for the aerosol relied on the external mixing of soluble and insoluble components, the estimates obtained here are suggestive only of magnitudes. Nonetheless, as the magnitudes prove to be comparable to those deduced from satellite imagery data, the example presented here could serve as a guide for obtaining more realistic estimates for the effects of clouds on the scattering of sunlight by aerosols. Estimating the enhancement in aerosol scattering requires both the changes in the aerosol scattering cross sections due to the increases in RH as clouds are approached and the probability of cloud-free distances to clouds for oceans. The probability of cloud-free distances to cloud was derived from CALIPSO lidar observations.

[26] Table 2 summarizes the relative humidity inferred from the INDOEX C-130 observations at various cloud-free distances to cloud and the expected increase in the aerosol scattering cross sections expressed as the ratio of the cross section to its value for a relative humidity far from clouds, distances $\geq$20 km. Seventy percent was taken to be a lower limit for the RH at cloud level associated with large cloud-free ocean regions, with changes in scattering cross sections as modeled earlier and depicted in Figure 5. The rise in relative humidity from distances $\geq$20 km to 1 km from cloud is likely to reflect a rise throughout the subcloud layer and consequently affects most of the particles in the cloud-free column. The value for the RH reported in the last kilometer to cloud is, as was noted earlier, probably reflective of only the RH at cloud level and thus only a fraction of particles are affected. Calculations were performed for the enhancement in the aerosol scattering cross section and the direct aerosol effect assuming that all of the particles within the last kilometer were affected and then with only a quarter of the particles affected.

[27] Table 3 combines the enhancements in scattering cross sections with the occurrences of cloud-free distances to clouds for ocean regions derived from the CALIPSO lidar observations. As it orbits the Earth, the lidar beam draws a pencil line on the ocean surface. The lengths of the cloud-free trajectories were used to estimate the sizes of the cloud-free areas assuming that the areas exhibit no preferred alignment with respect to the Earth's coordinate system. Large cloud-free ocean regions are relatively rare. Counting regions with cloud-free paths to clouds <50 km, the average distance obtained using the 300-m sampling and 70-m resolution of the CALIPSO lidar is 3.7 km. Sixty-six percent of the cloud-free regions are within 4 km of cloud and 31% are within 1 km. The distribution, however, has a long tail, with 8% having cloud-free paths to cloud >20 km.

Table 2. Cloud-Free Distances for Ocean Regions and the Corresponding RH and Ratio of Aerosol Scattering Cross Section to its Value at an RH of 70%, the Value Assumed at the Altitude of Low-Level Clouds For Large Cloud-Free Regions, Based on INDOEX Observations

Distance to Cloud (km)	RH (%)	Ratio of Scattering Cross Sections
0.1	95	2.49
1	90	1.69
4	90	1.69
20	70	1.0
>20	70	1.0

Table 3. Fractions of Cloud-Free Ocean Within a Given Distance of Cloud and the Associated Average RH, Average Ratio of Aerosol Scattering Cross Section, and Estimated Contribution to the Aerosol Direct Effect Normalized by the Effect for Large (>20 km) Cloud-Free Oceans

Distance to Cloud (km)	Fraction of Cloud-Free Ocean	Average RH (%)	Average Ratio of Scattering Cross Sections	Relative Contribution to Aerosol Direct Effect
1–0	0.31	93	2.17[a]	0.67[a]
4–1	0.35	90	1.69	0.59
20–4	0.26	80	1.20	0.31
>20	0.08	70	1.0	0.08
Net effect				1.65[a]

[a]The numbers given assume that the entire aerosol column is affected by the rise in humidity in the last kilometer. If only a quarter of the aerosol is affected, the average ratio of the scattering cross section becomes 1.81, the relative contribution to the direct effect becomes 0.56, and the net effect becomes 1.54.

[28] If the RH far from clouds is taken to be as low as 70% and the RH increases to 90% as clouds are approached, (i.e., from 20 km to 4 km, or since RH appeared to be constant in Figure 4a between 4 km and 1 km, from 20 km to 1 km), the increase in scattering cross sections accompanying the rise in RH for the INDOEX aerosol would be 69% at 4 km. The average RH for cloud-free regions 20 km to 4 km from cloud would be 80%, which for the INDOEX aerosol would result in a 20% enhancement in scattering cross section averaged across that distance. Similarly, capturing the rapid rise in RH from 1 to 0.1 km and then to saturation at cloud edge following the observations shown in Figure 4a, the average RH for the last kilometer would be 93%, for over a factor of 2 enhancement in average scattering cross section, if all the particles were affected by the rise in RH, but only a little over an 80% enhancement if a quarter of the particles were affected ($0.75 \times 1.69 + 0.25 \times 2.17 = 1.81$).

[29] Combining the averages of the RH and their associated enhancements in aerosol scattering cross sections with the occurrences of cloud-free distances to cloud for ocean regions leads to estimates of the relative contributions to the aerosol direct radiative effect (as given in the last column of Table 3). The relative contributions are given by $f(x)\sigma(x)/\sigma_{20}$, where $f(x)$ is the frequency of cloud-free ocean regions with size x within the interval between x and $x + dx$, $\sigma(x)$ is the scattering cross section associated with the cloud-free region, and σ_{20} is the scattering cross section for large (>20 km) cloud-free regions and is used as the basis for the relative contributions. The average enhancement is given by

$$\frac{\bar{\sigma}}{\sigma_{20}} = \int dx f(x) \frac{\sigma(x)}{\sigma_{20}} \approx \sum_i f_i \frac{\sigma_i}{\sigma_{20}}, \qquad (2)$$

where $\bar{\sigma}$ is the average scattering cross section for cloud-free oceans, and f_i and σ_i/σ_{20} are the associated frequencies and average ratio of scattering cross sections listed in Table 3 for the discrete form of the integral in (2). The cumulative effect of the enhancement, as given by $\bar{\sigma}/\sigma_{20}$ in (2), is 65% over the aerosol direct effect inferred for large cloud-free ocean regions, with slightly more than 40% of the contribution falling within a kilometer of clouds, assuming that all particles within the last kilometer to cloud are affected by the rise in RH. If only a quarter of the particles are affected, the enhancement is 54%, with slightly less than 40% of the enhancement falling within a kilometer of the clouds. As can be determined from the data given in Table 2, if at distances greater than 20 km the cloud-free air was taken to be at 80% RH instead of 70% RH, the net enhancement would be 45%, assuming that all the particles within the last kilometer were affected by the rise in RH and a 35% enhancement if only a quarter of the particles in the last kilometer were affected. Given the range of RH assumed for large cloud-free ocean regions (70–80%) and the range for the fraction of aerosols affected by the rise in RH for the last kilometer (25–100%) the range in enhancement becomes 35–65%.

[30] Estimates of the aerosol direct radiative effect based on MODIS [*Remer and Kaufman*, 2006] and CERES observations [*Loeb and Manalo-Smith*, 2005] include observations of cloud-free regions within about 1–2 km of cloud. Consequently, the effects due to the rise in relative humidity as well as those due to the illumination of cloud-free columns adjacent to clouds are present in such observations. For example, *Loeb and Manalo-Smith* [2005] used the CERES Single Satellite Footprint (SSF) data to study the dependence of retrieved aerosol optical depth on cloud cover fraction for Terra CERES fields of view. The CERES fields of view are approximately 20 km across at nadir. The SSF includes two sets of retrieved aerosol products, the MODIS MOD04 product, described by *Remer et al.* [2005], and an aerosol product developed by NOAA, the NOAA-SSF product, described by *Ignatov et al.* [2005]. The enhancement in the 0.64-μm aerosol optical depth is approximately 50% per unit cloud cover for the NOAA-SSF product and 90% per unit cloud cover for the MOD04 product for cloud cover fractions, A_C, within the CERES fields of view in the range of $0 \leq A_C \leq 0.95$. The difference in the rise is the result of the different methods used for cloud screening and the different methods used to obtain the aerosol products from the cloud-screened reflectances. The enhancements in optical depths are consistent with the upper limits of the enhancement estimated here for the increase in scattering cross sections due to the rise in RH as clouds are approached. Likewise the estimate reported here is consistent with the 60% enhancement in the 870 nm MODIS reflectances reported by *Koren et al.* [2007] for cloud-free oceans in going from 20 km to within 1 km of clouds.

[31] The enhancement in cloud-free radiances due to the presence of nearby clouds depends not only on the distance to clouds but also on cloud properties. Clouds with large amounts of liquid water and large reflectivities can be expected to have large effects on the nearby cloud-free

radiances through both the growth of aerosols resulting from the rise in RH near the cloud boundaries and the enhancement in the illumination of the cloud-free atmosphere. Thin, isolated, tenuous clouds can be expected to have little if any effect on either the RH or the illumination of the nearby cloud-free atmosphere. In addition, the results presented here were based on frequencies for cloud-free distances to cloud derived from CALIPSO lidar observations. The CALIPSO observations are highly sensitive to the presence of cloud, and consequently, their use in characterizing the sizes of cloud-free ocean regions clearly leads to an overestimate of the fraction of clouds likely to have significant effects on the aerosol, at the expense of an underestimate in the frequencies and sizes of cloud-free regions.

7. Conclusions

[32] This study revealed that on average, RH increases with proximity to low-level, small marine cumulus clouds in the Indian Ocean. The increase is from 88–90% at 1–4 km horizontal distance from the cloud to 94–96% at 100 m with a similar increase in the last 100 m. On the basis of the aerosol model used by *Rajeev et al.* [2000] for the composition of the INDOEX aerosol, hygroscopic growth due to this humidity field could cause a 40–80% increase in aerosol scattering cross sections within the last kilometer adjacent to clouds, assuming that all the particles in the last kilometer are affected by the rise in RH. The changes in scattering cross sections, however, would probably be confined to the levels near the cloud suggested to be approximately a quarter of the aerosol column on the basis of perusal of the INDOEX SABL lidar observations. For aerosols in the far field, where the RH could be substantially lower (70–80%), the changes in scattering cross sections in going to the proximity of clouds (1–4 km, 90% RH) would be as much as twice as large as that for the last kilometer from cloud edge. The changes in RH for the far field aerosol are likely to affect the entire column, whereas those in the last kilometer before cloud edge are likely to affect only the fraction of the column occupied by the clouds.

[33] Except for a 100-m region just before cloud, no significant changes in particle concentrations could be found in the INDOEX particle concentrations. Within the last 100 m, a possible rise in larger aerosols or cloud drop number was indicated, presumably as a result of the swelling of hygroscopic aerosol particles in the high-humidity air near clouds, making the particles detectable with the FSSP-300. The rise, however, could have also resulted from remnants of clouds that lacked sufficient droplet number and liquid water concentrations for the horizontal dimensions (~330 m) required of "in cloud" air in this study.

[34] In addition to the enhancement in scattering by aerosols due to the rise in RH near clouds, *Marshak et al.* [2008] have described how the illumination of cloud-free columns by the surrounding clouds causes an apparent increase in scattering attributed to aerosols by existing satellite retrieval schemes. At the same time, the illumination gives rise to an apparent increase in the retrieved concentration of fine-mode particles relative to that of coarse mode particles. They refer to the change in the spectral color of the scattered light as the "bluing of the aerosol," as much of the additional sunlight in the cloud-free columns is scattered by molecules. Here, observations with the MCR for two fairly representative cases indicated nearly a 50% enhancement in reflectances associated with the cloud-free ocean at both 0.64 and 1.06 μm under both heavy and light aerosol loadings beginning 1–2 km from cloud edge. The magnitude of the enhancement was comparable to that calculated for the fractional increase in the scattering cross section of the aerosol due to the rise in RH observed near clouds. In addition, the enhancements observed with the MCR were likely due to a combination of the larger cross sections resulting from the rise in RH and the enhanced illumination of the cloud-free regions adjacent to the clouds [*Wen et al.*, 2007; *Marshak et al.*, 2008].

[35] In any event, the results obtained here clearly identify an increase in RH and a consequent increase in particle growth and scattering cross sections as a potential mechanism for explaining increases in aerosol burdens with increasing cloud cover commonly reported in satellite-based studies of aerosol optical depths in cloudy regions [*Sekiguchi et al.*, 2003; *Ignatov et al.*, 2005; *Loeb and Manalo-Smith*, 2005; *Kaufman et al.*, 2005; *Matheson et al.*, 2006a; *Koren et al.*, 2007; *Quaas et al.*, 2008; *Loeb and Schuster*, 2008]. The increase in scattering cross sections due to the increase in relative humidity in cloudy regions is predicted to produce a 35–65% enhancement in the apparent scattering by aerosols in going from large cloud-free regions (>20 km scale) to cloud edges, with more than two thirds of the increase occurring within the last 4 km before cloud edge. As most of the cloud-free ocean regions (>90%) are smaller than 20 km, the rise in aerosol scattering due to the increase in humidity clearly needs to be accounted for in estimates of the aerosol direct radiative forcing.

[36] **Acknowledgments.** This work was funded by National Oceanic and Atmospheric Administration's Climate Program Office under Atmospheric Composition and Climate grant NA06OAR4310083 and by the CALIPSO Science Team under NASA grant NNX07AT11G. We also wish to thank the National Science Foundation and the crew of the NSF/NCAR C-130 aircraft for support and data acquired during the INDOEX program.

References

Albrecht, B. A. (1989), Aerosols, cloud microphysics and fractional cloudiness, *Science*, *245*, 1227–1230, doi:10.1126/science.245.4923.1227.

Baumgardner, D., J. E. Dye, R. G. Knollenberg, and B. W. Gandrud (1992), Interpretation of measurements made by the FSSP-300X during the Airborne Arctic Stratospheric Expedition, *J. Geophys. Res.*, *97*, 8035–8046.

Charlson, R. J., A. S. Ackerman, F. A.-M. Bender, T. L. Anderson, and Z. Liu (2007), On the climate forcing consequences of the albedo continuum between cloudy and clear air, *Tellus, Ser. B*, *59*, 715–727, doi:10.1111/j.1600-0889.2007.00297.x.

Clarke, A. D., S. Howell, P. K. Quinn, T. S. Bates, J. A. Ogren, E. Andrews, A. Jefferson, and A. Massling (2002), INDOEX aerosol: A comparison and summary of chemical, microphysical, and optical properties observed from land, ship, and aircraft, *J. Geophys. Res.*, *107*(D19), 8033, doi:10.1029/2001JD000572.

Feingold, G., and B. Morley (2003), Aerosol hygroscopic properties as measured by lidar and comparison with in situ measurements, *J. Geophys. Res.*, *108*(D11), 4327, doi:10.1029/2002JD002842.

Friehe, C. A., R. L. Grossman, and Y. Pann (1986), Calibration of an airborne Lyman-alpha hygrometer and measurement of water vapor flux using a thermoelectric hygrometer, *J. Atmos. Oceanic Technol.*, *3*, 299–304, doi:10.1175/1520-0426(1986)003<0299:COAALA>2.0.CO;2.

Hess, M., P. Koepke, and I. Schult (1998), Optical properties of aerosols and clouds: The software package OPAC, *Bull. Am. Meteorol. Soc.*, *79*, 831–844, doi:10.1175/1520-0477(1998)079<0831:OPOAAC>2.0.CO;2.

Hoppel, W. A., G. M. Frick, and R. E. Larson (1986), Effect of nonprecipitating clouds on the aerosol size distribution in the marine boundary layer, *Geophys. Res. Lett.*, *13*, 125–128, doi:10.1029/GL013i002p00125.

Ignatov, A., P. Minnis, N. Loeb, B. Wielicki, W. Miller, S. Sun-Mack, D. Tanré, L. Remer, I. Laszlo, and E. Geier (2005), Two MODIS aerosol products over ocean on the Terra and Aqua CERES SSF datasets, *J. Atmos. Sci.*, *62*, 1008–1031, doi:10.1175/JAS3383.1.

Kaufman, Y. J., and R. S. Fraser (1997), The effect of smoke particles on clouds and climate forcing, *Nature*, *277*, 1636–1639.

Kaufman, Y. J., and T. Nakajima (1993), Effect of Amazon smoke on cloud microphysics and albedo—Analysis from satellite imagery, *J. Appl. Meteorol.*, *32*, 729–744, doi:10.1175/1520-0450(1993)032<0729:EOASOC>2.0.CO;2.

Kaufman, Y. J., I. Koren, L. A. Remer, D. Rosenfeld, and Y. Rudich (2005), The effect of smoke, dust, and pollution aerosol on shallow cloud development over the Atlantic Ocean, *Proc. Natl. Acad. Sci. U. S. A.*, *102*, 11,207–11,212, doi:10.1073/pnas.0505191102.

Koren, I., L. A. Remer, Y. J. Kaufman, Y. Rudich, and J. V. Martins (2007), On the twilight zone between clouds and aerosols, *Geophys. Res. Lett.*, *34*, L08805, doi:10.1029/2007GL029253.

Loeb, N. G., and N. Manalo-Smith (2005), Top-of-atmosphere direct radiative effect of aerosols over global oceans from merged CERES and MODIS observation, *J. Clim.*, *18*, 3506–3526, doi:10.1175/JCLI3504.1.

Loeb, N. G., and G. L. Schuster (2008), An observational study of the relationship between cloud, aerosol and meteorology in broken low-level cloud conditions, *J. Geophys. Res.*, *113*, D14214, doi:10.1029/2007JD009763.

Lu, M.-L., J. Wang, A. Freedman, H. H. Jonsson, R. C. Flagan, R. A. McClatchey, and J. H. Seinfeld (2003), Analysis of humidity halos around trade wind cumulus clouds, *J. Atmos. Sci.*, *60*, 1041–1059, doi:10.1175/1520-0469(2003)60<1041:AOHHAT>2.0.CO;2.

Luderer, G., J. A. Coakley Jr., and W. R. Tahnk (2005), Using Sun glint to check the relative calibration of reflected spectral radiances, *J. Atmos. Oceanic Technol.*, *22*, 1480–1493.

Marshak, A., G. Wen, J. A. Coakley Jr., L. A. Remer, N. G. Loeb, and R. F. Cahalan (2008), A simple model for the cloud adjacency effect and the apparent bluing of aerosols near clouds, *J. Geophys. Res.*, *113*, D14S17, doi:10.1029/2007JD009196.

Matheson, M. A., J. A. Coakley Jr., and W. R. Tahnk (2005), Aerosol and cloud property relationships for summertime stratiform clouds in the northeastern Atlantic from AVHRR observations, *J. Geophys. Res.*, *110*, D24204, doi:10.1029/2005JD006165.

Matheson, M. A., J. A. Coakley Jr., and W. R. Tahnk (2006a), Multiyear Advanced Very High Resolution Radiometer observations of summertime stratocumulus collocated with aerosols in the northeastern Atlantic, *J. Geophys. Res.*, *111*, D15206, doi:10.1029/2005JD006890.

Matheson, M. A., J. A. Coakley Jr., and W. R. Tahnk (2006b), Effects of threshold retrievals on estimates of the aerosol indirect radiative forcing, *Geophys. Res. Lett.*, *33*, L07705, doi:10.1029/2005GL025614.

Nakajima, T., A. Higurashi, K. Kawamoto, and J. E. Penner (2001), A possible correlation between satellite-derived cloud and aerosol microphysical parameters, *Geophys. Res. Lett.*, *28*, 1171–1174, doi:10.1029/2000GL012186.

Podgorny, I. A. (2003), Three-dimensional radiative interactions in a polluted broken cloud system, *Geophys. Res. Lett.*, *30*(14), 1771, doi:10.1029/2003GL017287.

Quaas, J., O. Boucher, and F.-M. Bréon (2004), Aerosol indirect effects in POLDER satellite data and the Météorologie Dynamique—Zoom (LMDZ) general circulation model, *J. Geophys. Res.*, *109*, D08205, doi:10.1029/2003JD004317.

Quaas, J., O. Boucher, N. Bellouin, and S. Kinne (2008), Satellite-based estimate of the direct and indirect aerosol climate forcing, *J. Geophys. Res.*, *113*, D05204, doi:10.1029/2007JD008962.

Radke, L. F., and P. V. Hobbs (1991), Humidity and particle fields around some small cumulus clouds, *J. Atmos. Sci.*, *48*, 1190–1193, doi:10.1175/1520-0469(1991)048<1190:HAPFAS>2.0.CO;2.

Rajeev, K., V. Ramanathan, and J. Meywerk (2000), Regional aerosol distribution and its long-range transport over the Indian Ocean, *J. Geophys. Res.*, *105*, 2029–2043, doi:10.1029/1999JD900414.

Ramanathan, V., et al. (2001), Indian Ocean experiment: An integrated analysis of the climate forcing and effects of the great Indo-Asian haze, *J. Geophys. Res.*, *106*, 28,371–28,398, doi:10.1029/2001JD900133.

Remer, L. A., and Y. J. Kaufman (2006), Aerosol direct radiative effect at the top of the atmosphere over cloud free ocean derived from four years of MODIS data, *Atmos. Chem. Phys.*, *6*, 237–253.

Remer, L. A., et al. (2005), The MODIS aerosol algorithm, products, and validation, *J. Atmos. Sci.*, *62*, 947–973, doi:10.1175/JAS3385.1.

Schanot, A. J. (1987), An evaluation of the uses and limitations of the Lyman-alpha hygrometer as an operational airborne humidity sensor, paper presented at 6th Symposium on Meteorological Observations and Instrumentation, Am. Meteorol. Soc., New Orleans, La.

Sekiguchi, M., T. Nakajima, K. Suzuki, K. Kawamoto, A. Higurashi, D. Rosenfeld, I. Sano, and S. Mukai (2003), A study of the direct and indirect effects of aerosols using global satellite data sets of aerosol and cloud parameters, *J. Geophys. Res.*, *108*(D22), 4699, doi:10.1029/2002JD003359.

Strapp, J. W., W. R. Leaitch, and P. S. K. Liu (1992), Hydrated and dried aerosol-size-distribution measurements from Particle Measuring Systems FSSP-300 probe and deiced PCASP-100X probe, *J. Atmos. Oceanic Technol.*, *9*, 548–555, doi:10.1175/1520-0426(1992)009<0548:HADASD>2.0.CO;2.

Twohy, C. H., et al. (2002), Deep convection as a source of new particles in the midlatitude upper troposphere, *J. Geophys. Res.*, *107*(D21), 4560, doi:10.1029/2001JD000323.

Weber, R. J., A. D. Clarke, M. Litchy, J. Li, G. Kok, R. D. Schillawski, and P. H. McMurry (1998), Spurious aerosol measurements when sampling from aircraft in the vicinity of clouds, *J. Geophys. Res.*, *103*, 28,337–28,346, doi:10.1029/98JD02086.

Wen, G., A. Marshak, R. F. Cahalan, L. A. Remer, and R. G. Kleidman (2007), 3D Aerosol-cloud radiative interaction observed in collocated MODIS and ASTER images of cumulus cloud fields, *J. Geophys. Res.*, *112*, D13204, doi:10.1029/2006JD008267.

Wetzel, M. A., and L. L. Stowe (1999), Satellite-observed patterns in stratus microphysics, aerosol optical thickness, and shortwave radiative forcing, *J. Geophys. Res.*, *104*, 31,287–31,299, doi:10.1029/1999JD900922.

Winker, D., M. Vaughan, and W. Hunt (2006), The CALIPSO mission and initial results from CALIOP, *Proc. SPIE*, *6409*, 640902, doi:10.1117/12.698003.

J. A. Coakley Jr., W. R. Tahnk, and C. H. Twohy, College of Oceanic and Atmospheric Sciences, Oregon State University, Corvallis, OR 97331-5503, USA. (twohy@coas.oregonstate.edu)